JOURNAL OF MATERIALS SCIENCE **35** (2000) 3997–4007

High temperature behaviour of yttrium implanted pure iron and extra low carbon steel

E. CAUDRON*, H. BUSCAIL, F. RIFFARD
Laboratoire Vellave d'Elaboration et d'Etude des Matériaux, Equipe Locale Université Blaise Pascal Clermont-Fd II, B.P. 219, 43006 Le Puy en Velay, France
E-mail: Caudron@IUTSUX01.u-clermont1.fr

High temperature behaviour of yttrium implanted pure iron and extra low carbon steel were analyzed at $T = 700^{\circ}$C and under oxygen partial pressure $P_{O2} = 0.04$ Pa for 24 h to show the benefit of yttrium incorporation to the improvement of the implanted sample corrosion resistance at high temperature. Compositions and structures of yttrium implanted and unimplanted samples were investigated prior to high temperature oxidation studies by several analytical and structural techniques (RBS, RHEED and XRD) to observe the initial yttrium implantation depth profiles in the specimens. High temperature oxidation tests performed by thermogravimetry and by *in-situ* high temperature X-ray diffraction were carried out with the same experimental conditions on yttrium implanted and unimplanted samples to have reference analyses. The aim of this paper is to show the initial nucleation stage of the main compounds induced by oxidation at high temperature according to the initial sample treatment. The results obtained by *in-situ* high temperature X-ray diffraction will be compared to those by thermogravimetry to show the existing correlation between weight gain curves and structural studies. Our results allow to understand the improved corrosion resistance of yttrium implanted pure iron and extra low carbon steel at high temperature.

1. Introduction

The protection of high temperature pure iron and steels against oxidation is one of the most interesting technological subjects investigated nowadays because of its potential industrial applications. Numerous methods based on protective coatings obtained by several techniques (CVD, PVD, sol-gel methods,...) were studied to improve alloy corrosion resistance at high temperature. Another solution to obtain protective oxide scale is ion implantation which allows to incorporate a controlled concentration of oxygen reactive elements such as cerium, yttrium or hafnium into studied materials [1–13]. However the adherence of the scale to these alloys during service is necessary to maintain oxidation resistance at high temperature. The aim of this study is to characterize the main compound growths in yttrium implanted and unmiplanted pure iron and extra low carbon steel samples induced during oxidation test at high temperature. The experimental conditions used in thermogravimetry and *in-situ* high temperature analyses (i.e. $T = 700^{\circ}$C and $P_{O2} = 0.04$ Pa for 24 h) were chosen on the one hand to avoid the transformation of the initial ferrite to austenite phase and on the other hand to ensure formation of one of the most current corrosions product namely wustite (FeO).

2. Experimental details

The compositions of pure iron and extra low carbon steel samples investigated in this study obtained using inductively-coupled plasma mass spectrometry (ICPMS) are given in Table I. Rectangular specimens (surface area of around 3 cm^2 and 1 mm thick) are abraded with up to 1200-grit SiC paper, polished with 0.3 μm diamond paste, degreased with acetone and dried. This surface preparation is followed by yttrium implantation performed using a 180 keV energy beam (current : 30–35 mA) corresponding to a nomimal dose of 10^{17} ions/cm^2 by sample surface scanning using a 0.5 mm ion beam diameter for 106 min. to obtain the whole surface implantation.

The yttrium depth distributions before high temperature oxidation test in pure iron and extra low carbon steel were investigated by Rutherford backscattering spectrometry (RBS) using an alpha beam energy of 1.8 MeV at normal incidence on the sample with a beam current in the 10–50 nA range. The alpha backscattered particles were detected at 160° with a 25 mm^2 Si(Li) detector at a distance of 100 mm. We have used this nuclear analytical technique because we had previously reported its successful contribution in the case of sputtered thin film composition

* Author to whom all correspondence should be addressed.

TABLE I Chemical compositions (wt%) of pure iron and extra low carbon steel obtained by ICPMS

Sample	C	Mn	P	S	Si	Al	V	Fe
Fe	0.004	<0.001	<0.005	<0.002	<0.005	<0.005	<0.001	Bal
Fe-C	0.054	-	-	<0.001	-	-	-	Bal

determination [14–18]. These studies were completed by structural techniques such as reflection high energy electron diffraction (RHEED) using an incident electron beam of 100 keV and X-ray diffraction (XRD) using the Cu $K_{\alpha 1}$=1.5406 Å radiation. Analytical and structural techniques were also used on unimplanted samples to have reference analyses before yttrium implantation.

High temperature studies were performed for 24 h at 700°C and under controlled oxygen partial pressure (0.04 Pa) using a Setaram TGDTA 92-1600 microthermobalance for mass gain and a high temperature Anton PAAR HTK 1200 chamber with integrated sample spinner in a Philips X'pert MPD diffractometer for X-ray diffraction studies. *In-situ* X-ray diffraction analyses were performed, also using the Cu $K_{\alpha 1}$=1.5406 Å radiation, every hours to observe the behaviour of the main compounds induced after yttrium implantation and the initial nucleation stage of new compounds during high temperature oxidation studies. Thermogravimetry and X-ray diffraction techniques were also used on unimplanted samples to have reference analyses during high temperature oxidation studies.

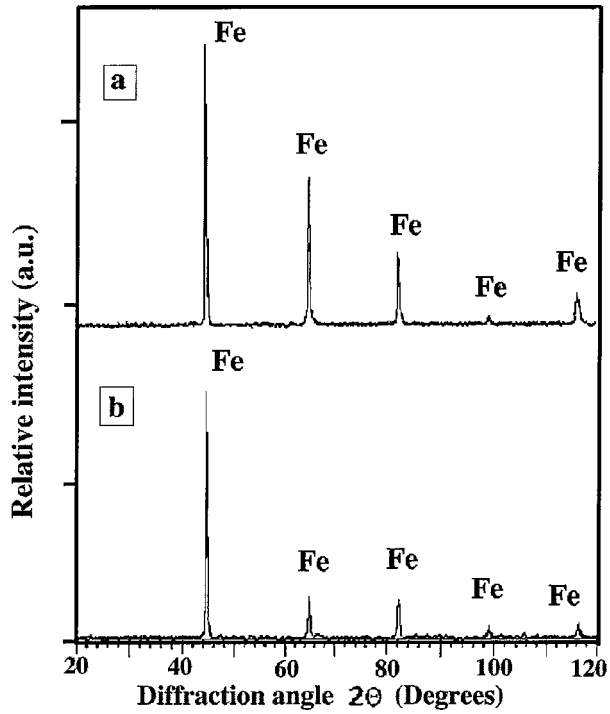

Figure 1 X.R.D. experimental spectra of unimplanted pure iron (a) and extra low carbon steel (b).

3. Results and discussion

3.1. Yttrium implantation effect on pure iron and extra low carbon steel prior to high temperature oxidation test

3.1.1. Initial samples characterization

Fig. 1 gives the XRD reference spectra obtained on pure iron (Fig. 1a) and extra low carbon steel (Fig. 1b). The two XRD spectra correspond to the same alpha-iron structure (JCPDS 06-696). The relative intensities observed for both samples indicate some preferred orientations of the initial substrates.

3.1.2. Yttrium implanted samples characterization

For RBS analysis three acquisitions on different points of the surface were performed for each sample to verify the homogeneity of yttrium implantation. Rutherford backscaterring spectrometry is one of the most powerful analytical techniques to determine yttrium depth profiles in our study because the implanted particle (yttrium) has a mass heavier than that of the substrate (pure iron or extra low carbon steel). The number of counts versus the energy of the backscattered particles gives us the yttrium distribution in the samples.

RBS experimental spectra obtained on pure iron and extra low carbon steel are given in Fig. 2 (RBS experimental spectra (plots) with their corresponding simulation (continuous line)). In both cases yttrium implantation corresponds to the signal extending from channel 380 to 440 and the Fe substrate signal (bulk signal) spreads from channel 100 to 380. The peaks observed in Fig. 2 near channel 390 are due to the overlapping of the yttrium peak with the substrate plateau. We have also tried to determine the oxygen depth profiles in the sample but with greater errors than in the case of yttrium because this light element has its characteristic peak on the Fe substrate plateau in the RBS spectra. Yttrium and oxygen depth distributions were processed using a modeling software (RUMP: Rutherford Universal Modeling Program) allowing the simulation of element concentrations according to the analyzed depth. The oxygen presence detected by RBS in yttrium implanted samples can be explained by the combination of three phenomena which are: the sputtering of the naturally oxidized sample surfaces during implantation process, the low oxygen partial pressure (lower than 10^{-2} Pa) existing in the implantation chamber and the sample heating (below 200 °C) observed during yttrium implantation treatment. For both pure iron and extra low carbon steel we have determined the resulting Y/Fe and O/Fe ratios to show the yttrium and oxygen depth profiles in the samples (ratios uncertainties are respectively $\Delta(Y/Fe) = \pm 0.01$ and $\Delta(O/Fe) = \pm 0.03$ and depth uncertainties $\Delta(\text{depth}) = \pm 2$ nm obtained after calculating RBS experimental standard mean deviations).

Fig. 3 gives the resulting Y/Fe and O/Fe ratios obtained by RBS concerning the yttrium and oxygen depth distributions in pure iron (Fig. 3a) and extra low carbon steel (Fig. 3b). The results obtained on pure iron (Fig. 3a) show that yttrium penetrates as deep as about 120 nm and has its maximum concentration at a depth

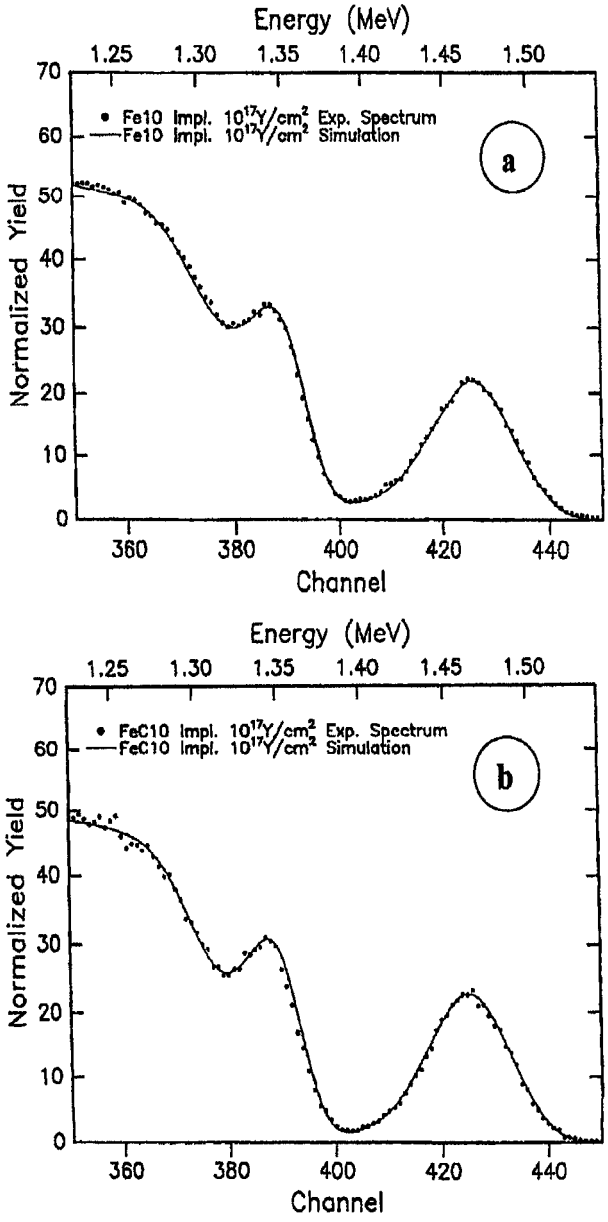

Figure 2 RBS spectrum enlargement showing implanted yttrium depth profiles of pure iron (a) and extra low carbon steel (b) (experimental spectrum (plots) and corresponding simulation (continuous line)).

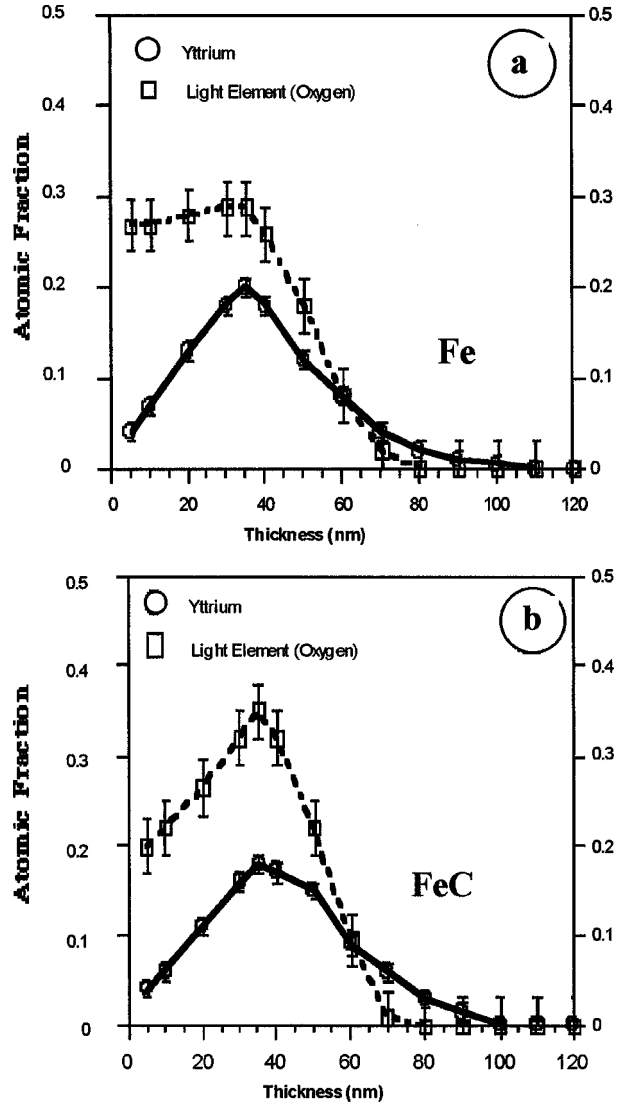

Figure 3 Comparison of yttrium and oxygen depth profiles in pure iron (a) and extra low carbon steel (b) obtained after calculating RBS experimental standard mean deviations. (ΔY/Fe) = $\pm$0.01; Δ(O/Fe) = $\pm$0.03 and Δ(depth) = $\pm$2 nm).

of 35 nm. The most interesting result concerns the fact that the oxygen depth profile displays a similar curve to that of yttrium. The O/Fe and Y/Fe ratio evolutions suggest the formation of several oxides in relation to yttrium implantation depth. For the lowest yttrium depth implantations (as deep as 35 nm) O/Y resulting ratios are in the range of 7 to 1.5. This ratio evolution seems to suggest that the formation of new compounds closely depends on the yttrium depth distribution in pure iron. It is important to note that O/Y ratio obtained at a depth of 35 nm corresponds to the composition of a stable yttrium oxide : Y_2O_3. Some authors [19–21] have reported that Y_2O_3 promotes the corrosion resistance of Cr_2O_3 and Al_2O_3 protective coatings against corrosive environments. Our results seem to indicate that yttrium implantation induces this Y_2O_3 compound formation inside the substrate before oxidation. Interestingly enough, Fig. 3a shows an important oxygen decrease after this 35 nm depth corresponding to the Y_2O_3 maximum concentration. These results allow us to conclude that the formation of this compound limits substantially the oxygen diffusion in the substrate. For the largest depths (above some 80 nm) Fig. 3a shows that oxygen is not present at these depths, there is only implanted yttrium in the pure iron structure.

The Y/Fe and O/Fe ratios obtained by RBS concerning the yttrium and oxygen depth profiles in extra low carbon steel (Fig. 3b) show that similar conclusions may be drawn concerning extra low carbon steel compared to pure iron : yttrium is to be found as deep as 120 nm; yttrium concentration reaches a maximum at 35 nm corresponding to the Y_2O_3 compound; oxygen and yttrium distribution curves are similar. However, it is important to note that O/Fe and O/Y ratios near the surface are lower than those observed in pure iron. These results seem to suggest that yttrium implantation promotes much more oxidized compounds in the case of pure iron.

Fig. 4a gives an XRD spectrum of the yttrium implanted pure iron sample. XRD analysis shows the presence of additional characteristic peaks corresponding to three structures which are Y_2O_3 (JCPDS 41-1105), $Y_3Fe_5O_{12}$ (JCPDS 43-507) and $FeYO_3$ (JCPDS

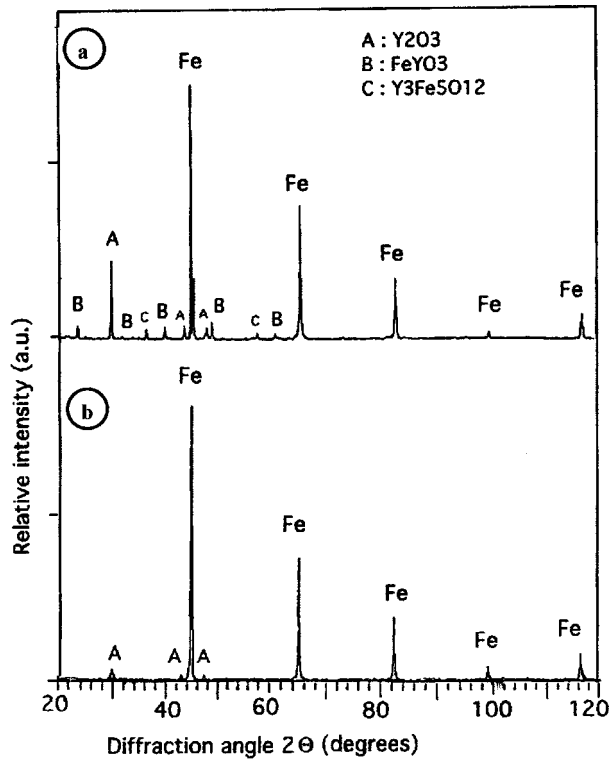

Figure 4 X.R.D. experimental spectra of yttrium implanted pure iron (a) and extra low carbon steel (b).

39-1489). The comparison of the different XRD peaks indicates that Y_2O_3 is the predominating yttrium oxide promoted by yttrium implantation. RHEED, a more sensitive surface technique than XRD, identified two compounds i.e. $Y_3Fe_5O_{12}$ (JCPDS 43-507) and $FeYO_3$ (JCPDS 39-1489) (Table II). The different structural techniques used in our study do not show the formation of iron oxides involved by yttrium implantation in the case of pure iron which might be accounted for by very low nanocrystalline phase concentrations and/or possible presence of amorphous compounds.

RHEED analysis performed on extra low carbon steel identified mainly the α-Fe (JCPDS 06-696) and FeO (JCPDS 06-615) structures (Table III) whereas XRD analyses (Fig. 4b) show only the Y_2O_3 structure

TABLE II RHEED results on yttrium implanted pure iron (100 keV incident electron beam)

d_{hkl} (Å) *Exp. values*	$Y_3Fe_5O_{12}$ (cubic - Ia3d) (JCPDS 43-507)		$FeYO_3$ (orthorhombic - Pnma) (JCPDS 39-1489)	
	d_{hkl}	*(hkl)*	d_{hkl}	*(hkl)*
3.42			3.43	(111)
3.09	3.09	(400)		
2.78	2.77	(420)	2.80	(200)
2.71			2.71	(121)
2.63			2.64–2.62	(002) - (210)
2.52	2.53	(422)		
2.27	2.26	(521)	2.28	(112)
1.91			1.92–1.90	(202)-(040)
1.72	1.72	(640)	1.71	(311)
1.63	1.65	(642)		
1.54	1.55	(800)	1.57 – 1.54 – 1.53	(240) - (042) - (123)
1.36	1.38–1.35	(840) - (842)	1.35	(242)
1.14	1.15	(864)		

TABLE III RHEED results on yttrium implanted extra low carbon steel (100 keV incident electron beam)

d_{hkl} (Å) *Exp. values*	α-Fe (cubic - Im3m) (JCPDS 6-696)		FeO (wustite) (cubic - Fm3m) (JCPDS 6-615)	
	d_{hkl}	*(hkl)*	*dhkl*	*(hkl)*
2.48			2.49	(111)
2.15			2.15	(200)
2.03	2.03	(110)		
1.52			1.52	(220)
1.42	1.43	(200)		
1.29			1.30	(311)
1.22			1.24	(222)
1.15	1.17	(211)		
1.08			1.08	(400)
1.00	1.01	(220)	0.99	(331)
0.94	0.92	(013)	0.96	(420)
0.83	0.83	(222)		
0.75	0.77–0.72	(123) - (004)		

(JCPDS 41-1105). These structural analyses seem to suggest that the Y_2O_3 compound is present at various amounts in the sample but appears to concentrate at the greater depths whereas FeO compound is rather located near the surface. These results can explain the O/Y ratios higher than 1.5 obtained by RBS at the lowest depths in both pure iron and extra low carbon steel. However the high O/Y ratios observed by RBS may also be attributed to some amorphous yttrium and/or iron and/or yttrium-iron oxides not detectable by structural techniques.

RBS, RHEED and XRD results suggest that the most highly oxidized compounds are mainly located near the surface whereas Y_2O_3 prevails around 35 nm. Moreover the formation of these new compounds can be attributed to the higher oxygen affinity of yttrium compared to that of iron and to the low oxygen partial pressure and temperature during the yttrium implantation process which can limit the growth of iron oxides. However it is important to note that yttrium implanted pure iron clearly shows a more important surface alteration than yttrium implanted extra low carbon steel which may explain the very different features of the XRD spectra observed in Fig. 4a and b. This phenomenon can be attributed to the higher carbon content in extra low carbon steel compared to pure iron which seems to contribute to a higher hardness than pure iron.

3.2. Oxidation kinetics at high temperature

3.2.1. Pure iron oxidation kinetics at high temperature

Fig. 5 shows the weight gain versus time curves ($\Delta m/S = f(t)$) of unimplanted and yttrium implanted pure iron samples oxidized for 24 h at 700°C under oxygen partial pressure of 0.04 Pa. This figure shows that in the case of unimplanted sample the oxidation follows a linear regime (linear rate constant : $k_{l(Fe)} = (3.1 \pm 0.2) \times 10^{-4}$ mg·cm^{-2}·s^{-1}) all along the oxidation test whereas in the case of yttrium implanted sample a higher oxidation rate is observed during the first 4 hours followed by a linear behaviour (linear rate constant : $k_{l(YFe)} = (1.5 \pm 0.1) \times 10^{-4}$ mg·cm^{-2}·s^{-1}).

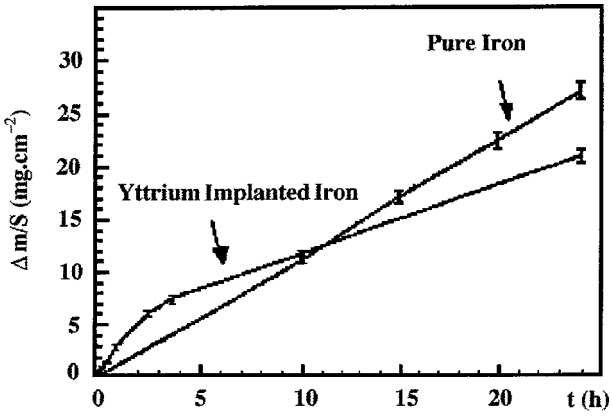

Figure 5 Weight gain versus time curves of unimplanted and yttrium implanted pure iron ($T = 700°C$; $P_{O2} = 0.04$ Pa).

Comparison between implanted and unimplanted sample weight gain curves indicates that a higher mass gain is observed during the first 10 hours for the implanted specimen, but after these first 10 hours the implanted sample exhibits a lower oxidation rate. The weight gain curve evolutions and the corresponding calculated oxidation linear rates underline the benefit of implanting yttrium into pure iron.

One interesting aspect of this study is the particular initial implanted sample oxidation regime observed during the first 4 hours which seems to contribute to a resulting better oxidation resistance at high temperature at the end of the oxidation test (as suggested by the corresponding linear oxidation rate). These results have prompted us to carry out *in-situ* high temperature X-ray diffraction studies to identify the main compounds promoting the higher oxidation rate during the first 4 hours on implanted specimens and the lower oxidation rate observed after these first 4 hours.

3.2.2. Extra low carbon steel oxidation kinetics at high temperature

The weight gain versus time curve ($\Delta m/S = f(t)$) of unimplanted and yttrium implanted extra low carbon steels oxidized for 24 h at 700°C under oxygen partial pressure of 0.04 Pa are given in Fig. 6. This figure shows that unimplanted sample weight gain curve exhibits two linear parts. In the early phase of the oxidation test (during the first 8 hours) an important linear weight gain is observed corresponding to a linear rate constant $k_1 = (2.8 \pm 0.2) \times 10^{-4}$ mg·cm^{-2}·s^{-1} followed by a second low linear oxidation rate (after 8 hours) with a smaller weight gain corresponding to a linear rate constant : $k_2 = (0.44 \pm 0.05) \times 10^{-4}$ mg·cm^{-2}·s^{-1}. The weight gain versus time curve ($\Delta m/S = f(t)$) of yttrium implanted extra low carbon steel oxidized for 24 h at 700°C under oxygen partial pressure of 0.04 Pa is also reported in Fig. 6 to have comparative analyses. This figure clearly shows the benefit of incorporating yttrium into extra low carbon steel because the resulting weight gain is lower than in the case of unimplanted sample. Moreover the weight gain curve exhibits in the early phase of the oxidation test a latent period of about 45 minutes during which no weight gain is observed. After this latent period the weight gain curve exhibits a parabolic regime with a parabolic rate constant $k_p = (0.51 \pm 0{,}04) \times 10^{-3}$ mg^2·cm^{-4}·s^{-1} corresponding to a lower weight gain than that observed in the case of unimplanted extra low carbon steel. These results have also prompted us to carry out high temperature *in-situ* X-ray diffraction analyses on the one hand to understand the two linear behaviours observed in the case of unimplanted sample and on the other hand the 45 minutes latent period and the low weight gain observed in the case of yttrium implanted sample by thermogravimetry.

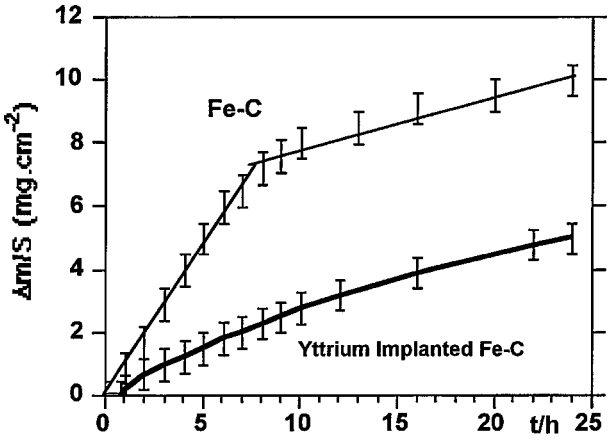

Figure 6 Weight gain versus time curves of unimplanted and yttrium implanted extra low carbon steel ($T = 700°C$; $P_{O2} = 0.04$ Pa).

3.3. *In-situ* high temperature X-ray diffraction characterization

3.3.1. Unimplanted and yttrium implanted pure iron in-situ high temperature X-ray diffraction characterization

In-situ high temperature X-ray characterization ($T = 700°C$; $P_{O2} = 0.04$ Pa) was performed every hours for 24 hours on both yttrium implanted and unimplanted pure iron (as reference analyses) samples. Initial unimplanted sample and the first 7 h *in-situ* oxidation test X-ray analyses are given in Fig. 7. This figure shows that the initial pure iron characteristic diffraction peaks (JCPDS 6-696) have completely disappeared during the first hour oxidation test in which FeO (wustite : JCPDS 6-615) and Fe_3O_4 (magnetite : JCDPS 19-629) are the two main compounds to be promoted. After the first hour small amounts of Fe_2O_3 (hematite : JCPDS 33-664) were also detected.

Comparison between the FeO, Fe_3O_4 and Fe_2O_3 typical characteristic peak intensities during the first 7 h oxidation test indicates the formation of a triple iron-oxide layer : FeO at the greatest depths, Fe_3O_4 at the lowest depths and Fe_2O_3 near the oxide-gaz interface. The Fe_3O_4 characteristic peak intensity increase is due to the formation of this compound on FeO at typical depths easily observable by X-ray diffraction. The characteristic peak intensities of the last compound induced by oxidation test i.e. Fe_2O_3 are very low which suggests the presence of a thin layer of this compound near the surface.

In-situ X-ray analyses performed between 6 h and 13 h clearly show the Fe_3O_4 layer growth during this oxidation test period (Fig. 8). Some representative X-ray

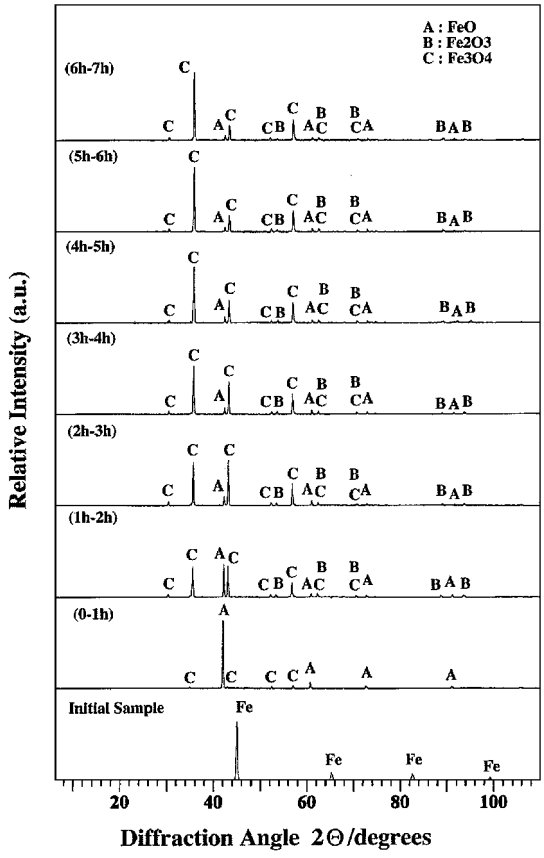

Figure 7 Initial sample and *in-situ* high temperature first 7 h XRD experimental spectra performed on unimplanted pure iron showing the main structures induced during high temperature oxidation test ($T = 700°C$; $P_{O2} = 0.04$ Pa).

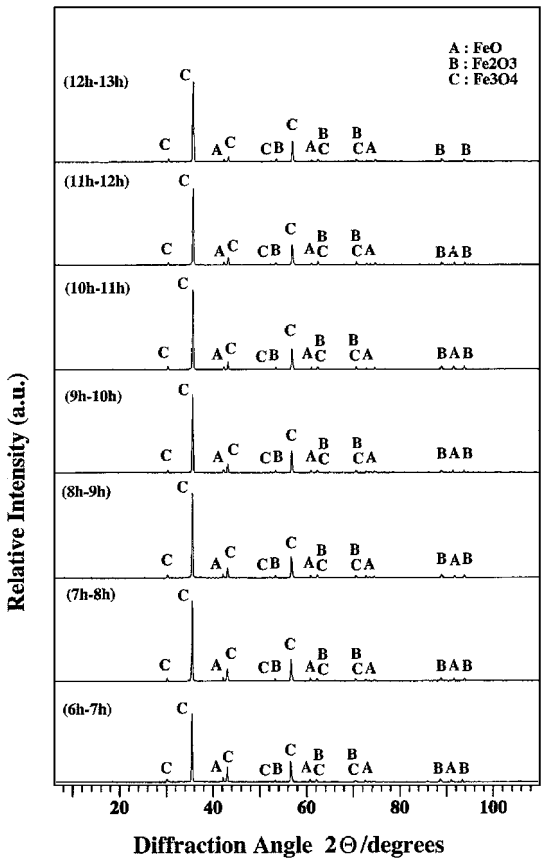

Figure 8 In-situ high temperature XRD experimental spectra performed on unimplanted pure iron showing the main structures induced during high temperature oxidation test between 6 h and 13 h ($T = 700°C$; $P_{O2} = 0.04$ Pa).

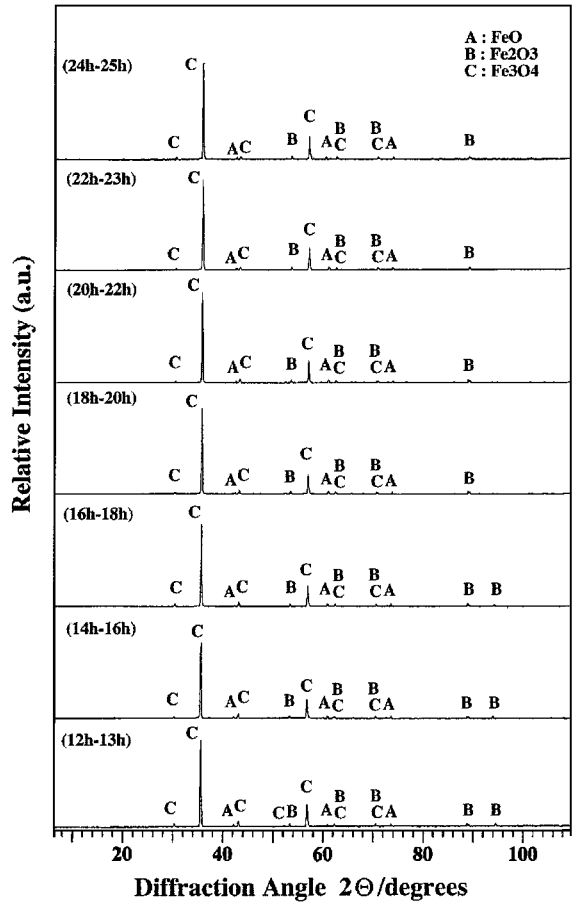

Figure 9 In-situ high temperature XRD experimental spectra performed on unimplanted pure iron showing the main structures induced during high temperature oxidation test between 12 h and 25 h ($T = 700°C$; $P_{O2} = 0.04$ Pa).

pure iron spectra obtained between 12 h and 25 h (Fig. 9) show that the wustite structure is present in the depths of the scale because its characteristic diffraction peaks become pratically undetectable after 24 hours of oxidation test.

Several theoretical models were suggested to explain the growth mechanism induced by diffusion during pure iron oxidation. In fact, wustite which can write as $Fe_{(1-x)}O$ is clearly deficient in iron and in early interpretations the defect structure being mainly due to single-iron vacancies [22–24]. It is now well established that wustite defect structure is in majority defect clusters resulting from iron vacancies and interstitials in a NaCl-type structure [25]. Concerning the diffusion mechanism the Wagner oxidation theory [22] based only on cationic vacancy movements in the case of $M_{(1-x)}O$ compounds is not sufficient when the oxidation induces the formation of multilayers. In fact, the Wagner model and other theories based on iron self-diffusion acting as an iron oxidation limiting step [26, 27] imply a parabolic oxidation regime not observed in our case. The oxidation behaviour observed in our study rather suggests that the scale-growth mechanism is limited by the adsorption rate of O_2 molecules on the oxide scale surface [13].

Initial yttrium implanted sample and the first 7 h *in-situ* oxidation test X-ray analyses are given in Fig. 10. This figure shows the important yttrium diffusion out of pure iron. In fact two compounds i.e. Fe_2YO_4 (JCPDS

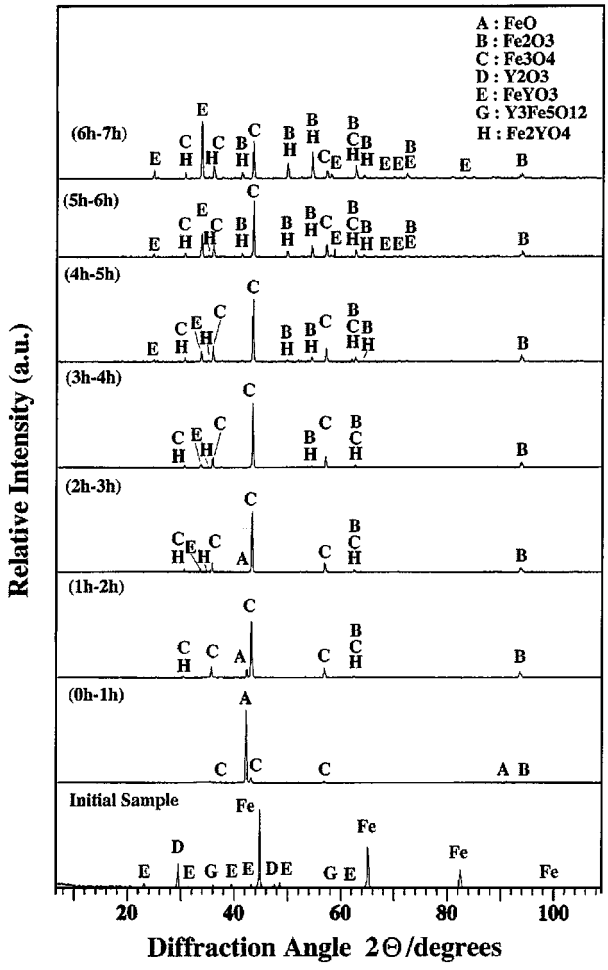

Figure 10 Initial sample and *in-situ* high temperature first 7 h XRD experimental spectra performed on yttrium implanted pure iron showing the main structures induced during high temperature oxidation test ($T = 700°C$; $P_{O2} = 0.04$ Pa).

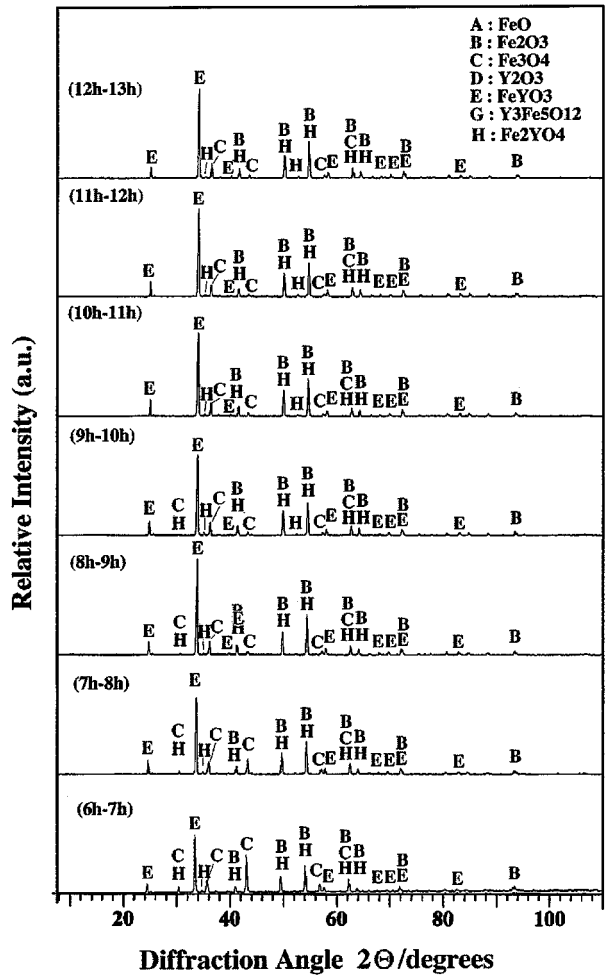

Figure 11 In-situ high temperature XRD experimental spectra performed on yttrium implanted pure iron showing the main structures induced during high temperature oxidation test between 6 h and 13 h ($T = 700°C$; $P_{O2} = 0.04$ Pa).

32-477) and $FeYO_3$ (JCPDS 39-1489) seem to be promoted along with the wustite, hematite and magnetite structures by the oxydation test. It is interesting to note that the main characteristic peaks of FeO structure decrease more rapidly in the case of yttrium implanted sample (Fig. 10) than in the case of unimplanted sample (Fig. 7).

In the same time Fe_2O_3, Fe_3O_4, $FeYO_3$ and Fe_2YO_4 seem to be the main structures involved by the oxidation test. The initial nucleation of the $FeYO_3$ structure may be explained by the transformation of the Y_2O_3 and Fe_2O_3 phases into $FeYO_3$ and the second yttrium-iron oxide formation may be accounted for the transformation of the Fe_3O_4 spinel-type structure combined with yttrium diffusion promoting the Fe_2YO_4 structure. These first X-ray analyses may be related to the first 4 hours weight gain curve behaviour observed by thermogravimetry (Fig. 5). The yttrium outward diffusion promotes the formation of mixed yttrium-iron oxides along with iron oxides typically observed on unimplanted sample which could lead to the high oxidation rate observed during this period.

In-situ high temperature XRD analyses performed between 6 h and 13 h are given in Fig. 11. This figure shows the formation of $FeYO_3$ and Fe_2YO_4 structures whereas FeO characteristic peaks were not detected and Fe_3O_4 characteristic peaks continue to decrease which seems to indicate that the formation of the yttrium-iron mixed oxides is mainly localized at the external interface. Some representative XRD spectra between 12 h and 25 h are given in Fig. 12 to show that no significant changes were observed during this period.

These results indicate that the formation of main compounds promoting the high temperature oxidation resistance is obtained after few hours (typically 2 or 3 hours) due to the high diffusion rate of yttrium. The evolution of $FeYO_3$ and Fe_2YO_4 characteristic peaks during the 24 h oxidation test seems to suggest that these compound growths are mainly localized at the gaz-oxide interface by outward yttrium diffusion through the oxide layer. After the initial nucleation stage of the two main yttrium-iron mixed oxides during the first 2 hours X-ray diffraction studies indicate the slow growth of these compounds which suggests the whole consumption of the implanted yttrium in the sample.

3.3.2. Unimplanted and yttrium implanted extra low carbon steel in-situ high temperature X-ray diffraction characterization

In-situ high temperature X-ray characterization analyses ($T = 700°C$; $P_{O2} = 0.04$ Pa) were performed every hours for 24 hours on unimplanted extra low carbon

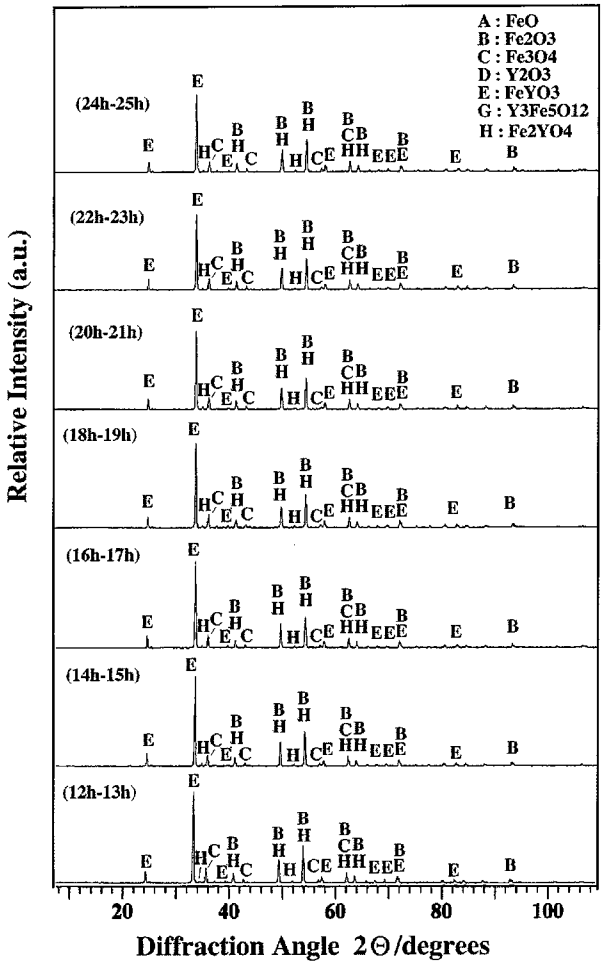

Figure 12 In-situ high temperature XRD experimental spectra performed on yttrium implanted pure iron showing the main structures induced during high temperature oxidation test between 12 h and 25 h ($T = 700°C$; $P_{O2} = 0.04$ Pa).

steel to observe the initial nucleation stage of the main compounds involved by oxidation test and to have reference analyses before examining yttrium implanted sample oxidation behaviour. Fig. 13 shows X-ray diffraction spectra of the initial sample (before oxidation) and the first 7 h *in-situ* high temperature oxidation test. This figure shows the important sample oxidation because iron characteristic diffraction peaks (JCPDS 6-696) have completely disappeared during the first hour oxidation test in which FeO (wustite : JCPDS 6-615) initial nucleation stage is observed. After the first hour the Fe_3O_4 structure (magnetite : JCDPS 19-629) is also detected whereas the Fe_2O_3 structure (hematite : JCPDS 33-664) is detected after 5 h.

In-situ X-ray analyses performed between 6 h and 13 h clearly show the Fe_3O_4 layer growth during this oxidation test period (Fig. 14). X-ray analyses performed between 6 h and 13 h also that the Fe_2O_3 characteristic peak intensities are very low which suggests the presence of this compound in the form of a thin layer near the surface as in the case of pure iron.

Comparison of the FeO, Fe_3O_4 and Fe_2O_3 typical characteristic peak intensities in Fig. 13 and Fig. 14 also seems to indicate the formation of a triple iron-oxide layer : FeO at the greatest depths, Fe_3O_4 at the lowest depths and Fe_2O_3 near the oxide-gas interface.

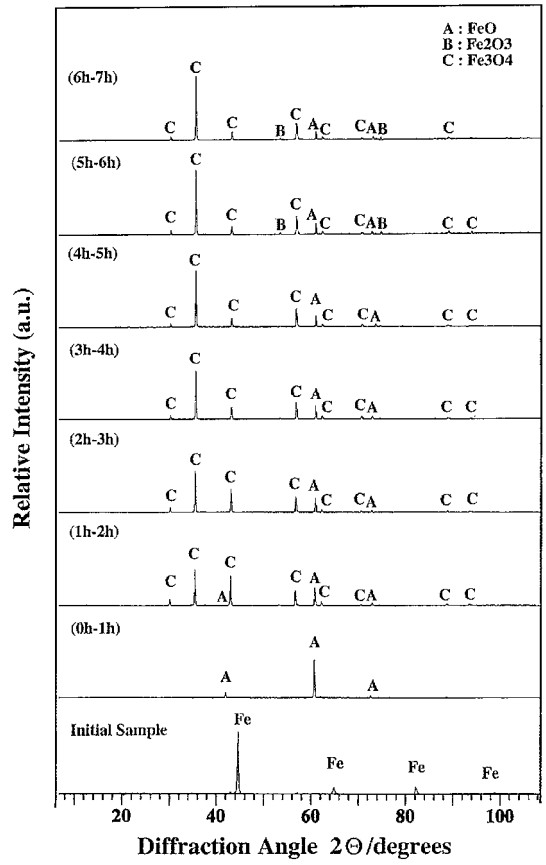

Figure 13 Initial sample and *in-situ* high temperature first 7 h XRD experimental spectra performed on unimplanted extra low carbon steel showing the main structures induced during high temperature oxidation test ($T = 700°C$; $P_{O2} = 0.04$ Pa).

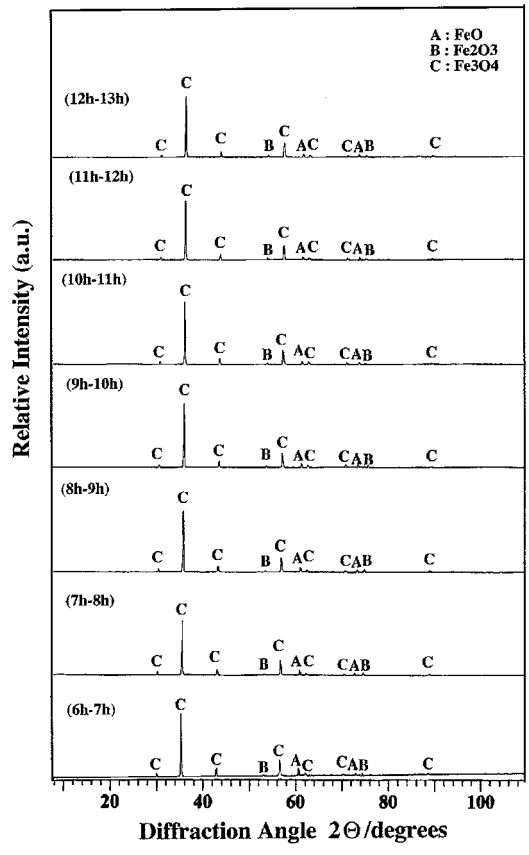

Figure 14 In-situ high temperature XRD experimental spectra performed on unimplanted extra low carbon steel showing the main structures induced during high temperature oxidation test between 6 h and 13 h ($T = 700°C$; $P_{O2} = 0.04$ Pa).

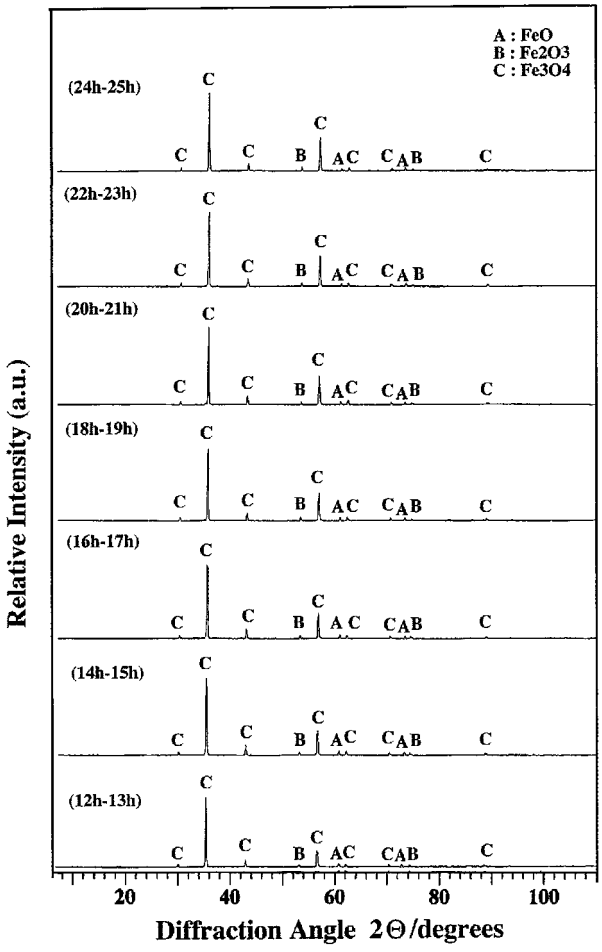

Figure 15 In-situ high temperature XRD experimental spectra performed on unimplanted extra low carbon steel showing the main structures induced during high temperature oxidation test between 12 h and 25 h ($T = 700°C$; $P_{O2} = 0.04$ Pa).

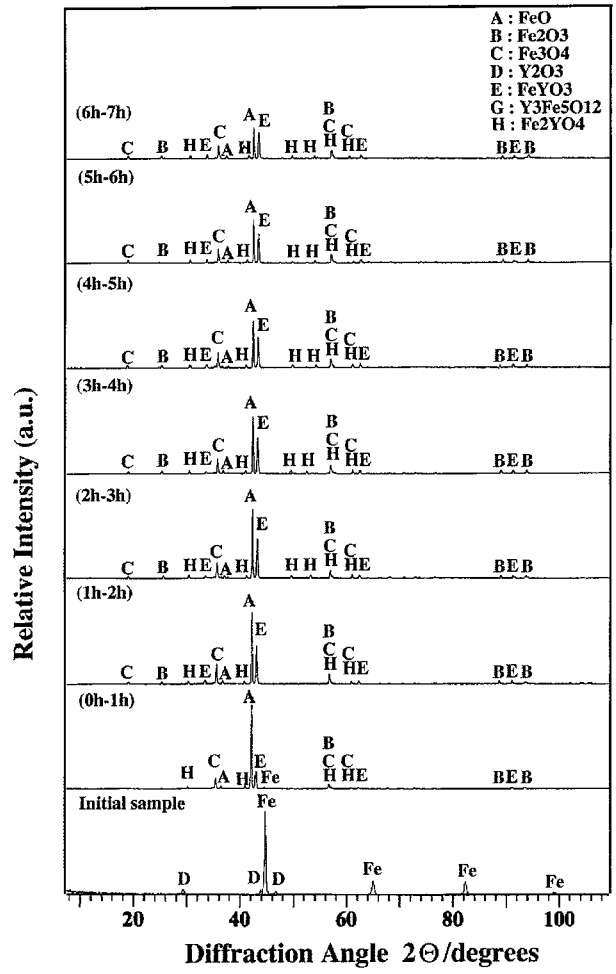

Figure 16 Initial sample and *in-situ* high temperature first 7 h XRD experimental spectra performed on yttrium implanted extra low carbon steel showing the main structures induced during high temperature oxidation test ($T = 700°C$; $P_{O2} = 0.04$ Pa).

The main representative X-ray analyses carried out between 12 h and 25 h are reported in Fig. 15. The results obtained in this figure confirm the previous observations : the FeO characteristic peaks become undetectable which clearly demonstrates the presence of this compound in the depths of extra low carbon steel. The Fe_3O_4 characteristic peaks clearly show the presence of this compound on the FeO layer and the Fe_2O_3 low characteristic intensity peaks suggesting the presence of this compound in the form of a thin layer on the surface of the sample.

The oxidation behaviour observed in our study also suggests that the scale-growth mechanism is mainly limited by the adsorption rate of O_2 molecules on the oxide scale surface as in the case of pure iron. Moreover it is important to note that carbon may also form some iron carbides which could limit the oxygen diffusion in steel as suggested by the variation in the linear oxidation rate observed in Fig. 6 but our X-ray analyses do not allow us to confirm this fact. However the concentrations of the iron carbide nanocrystalline phases may be below the detection limit of our XRD equipement.

High temperature *in-situ* X-ray diffraction analyses allow to observe and to understand the initial nucleation stages of the main compounds (i.e. FeO, Fe_3O_4 and Fe_2O_3) induced during the oxidation of extra low carbon steel. This first batch of results have prompted us to use this technique to observe the main compounds involved by oxidation in yttrium implanted extra low carbon steel.

X-ray diffraction spectra of the initial yttrium implanted sample (before oxidation) and the first 7 h *in-situ* high temperature oxidation test are given in Fig. 16. This figure suggests an important yttrium diffusion out of extra low carbon steel because the Y_2O_3 compound promoted by yttrium implantation has completely disappeared after the first hour of the oxidation test. The most interesting result is the fact that one iron characteristic peak was still observable after 1-hour oxidation whereas they were not observable after the first hour oxidation test in the case of unimplanted sample. These results could explain the 45-minute latent period observed in Fig. 6 during which no weight gain was detected for implanted sample and confirm the benefit of incorporating yttrium into extra low carbon steel to improve oxidation resistance at high temperature. Fig. 16 also shows that two main compounds i.e. $FeYO_3$ (JCPDS 39-1489) and Fe_2YO_4 (JCPDS 32-477) seem to be promoted along with the wustite, hematite and magnetite structures by the oxydation test. The formation of the two yttrium-iron oxides can be attributed to the high oxygen reactivity of yttrium which may promote these compounds as previously explained. The Fe_2YO_4

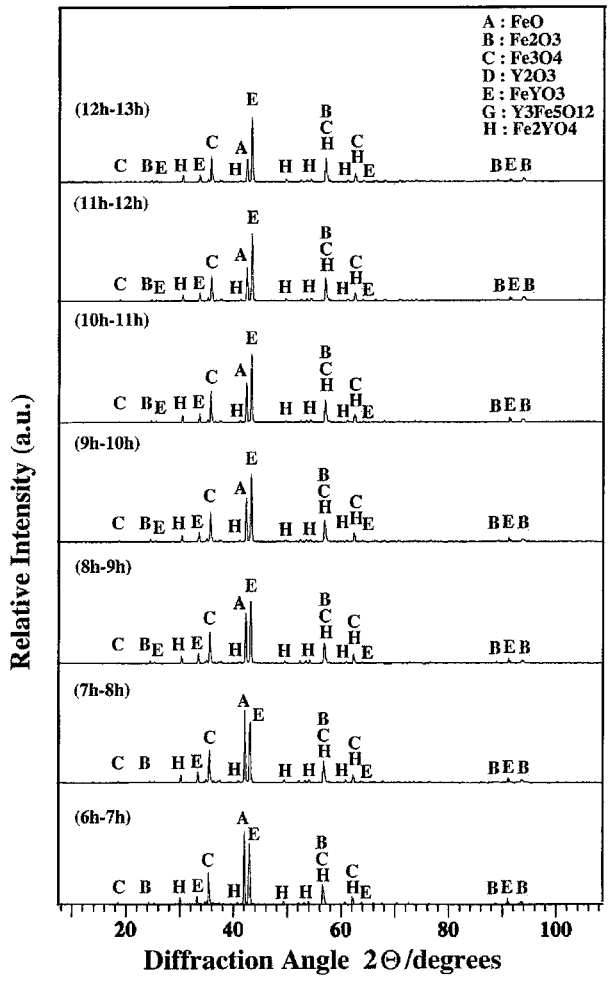

Figure 17 In-situ high temperature XRD experimental spectra performed on yttrium implanted extra low carbon steel showing the main structures induced during high temperature oxidation test between 6 h and 13 h ($T = 700°C$; $P_{O2} = 0.04$ Pa).

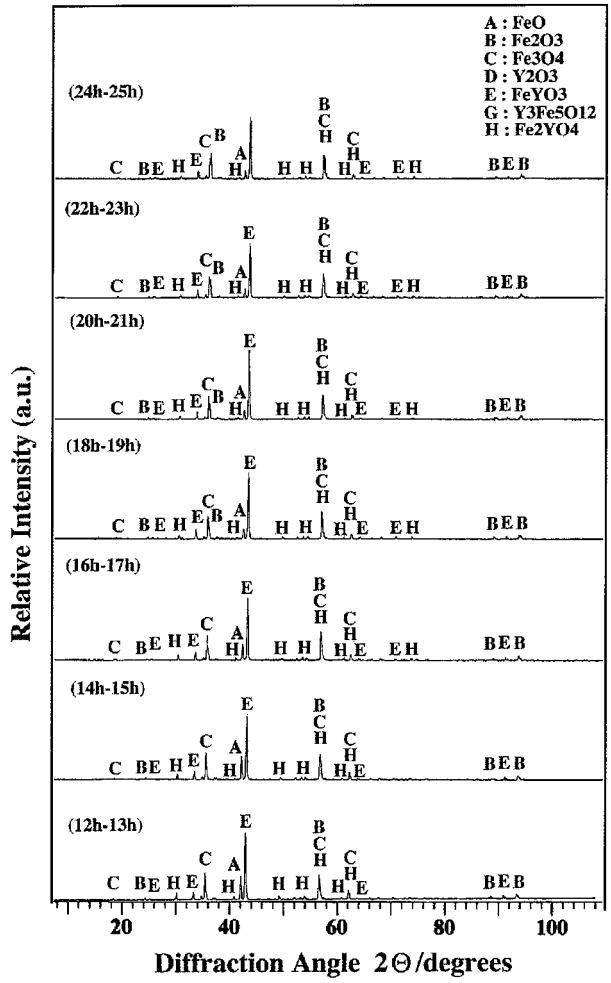

Figure 18 In-situ high temperature XRD experimental spectra performed on yttrium implanted extra low carbon steel showing the main structures induced during high temperature oxidation test between 12 h and 25 h ($T = 700°C$; $P_{O2} = 0.04$ Pa).

formation is of some importance because several authors have previously reported the anticorrosion properties of this compound at high temperature [19, 20].

In-situ high temperature XRD analyses performed between 6 h and 13 h are given in Fig. 17. This figure shows the formation of $FeYO_3$ and Fe_2YO_4 structures whereas FeO and Fe_3O_4 characteristic peaks continue to decrease which seems to indicate that the formation of yttrium-iron mixed oxides is also located at the external interface as in the case of yttrium implanted pure iron.

Some representative XRD spectra between 12 h and 25 h are given in Fig. 18 to show that no significant changes were observed during this period. These results indicate that the formation of the main compounds promoting high temperature oxidation resistance is also obtained quite rapidly due to the high diffusion rate of yttrium as observed for yttrium implanted pure iron. The protective character of the two main yttrium-iron oxides is underlined by the 45-minute latent period observed by thermogravimetry and the corresponding X-ray spectra with iron characteristic peak still observed during the first hour of oxidation test. After the initial nucleation stage of the two main yttrium-iron mixed oxides, X-ray diffraction studies indicate the slow growth of these compounds until all the yttrium implanted into the sample has been used up as in the case of yttrium implanted pure iron.

4. Conclusion

This study shows the different yttrium implantation effects on pure iron and extra low carbon steel. In both tested materials, yttrium implantations spread to the same depth (120 nm) and exhibit concentration maxima near 35 nm with oxygen depth profile curves similar to those of yttrium. However, extra low carbon steel seems to be less sensitive to yttrium implantation than pure iron on which the formation of several yttrium iron mixed oxides is observed. On pure iron, $Y_3Fe_5O_{12}$ and $FeYO_3$ compounds seem to prevail near the iron surface whereas Y_2O_3 appears to be prevalent at the greater depths. Yttrium implantation on extra low carbon steels seems mainly to promote the formation of Y_2O_3 (over the whole yttrium implanted depth range) and FeO (near the surface). The most interesting result is the fact that in both samples Y_2O_3 is the main compound formed using yttrium implantation. This study also shows the successful contribution of *in-situ* high temperature X-ray diffraction technique to the observation and understanding of the initial oxidation stage of unimplanted and yttrium implanted

samples observed by thermogravimetry. The most interesting high temperature X- ray diffraction result lies in that yttrium implantation promotes the formation of protective yttrium-iron mixed oxides at the external interface by outward yttrium diffusion through over the whole scale. These results underline that yttrium implantation offers a new possibility of increasing pure iron and extra low carbon steel corrosion resistances at high temperature.

References

1. P. MAYER and W. W. SMELTZER, *J. Electrochem. Soc.* **119** (1972) 626.
2. I. M. ALLAM, D. P. WHITTLE and J. STRINGER, *Oxid. Met.* **12** (1978) 35.
3. J. STRINGER, *Mat. Sci. Eng.* **A120** (1989) 129.
4. F. I. WEI and F. H. STOTT, *Corros. Sci.* **29** (1989) 839.
5. S. K. MITRA, S. K. ROY and S. K. BOSE, *Oxid. Met.* **34** (1990) 101.
6. J. JEDLINSKI, *Corros. Sci.* **35** (1993) 863.
7. Y. IKEDA and M. YATA, *J. Phys. IV* **9** (1993) 257.
8. Y. SAITO, B. ONAY and T. MARUYAMA, *ibid.* **3** (1993) 217.
9. H. BUSCAIL, P. SOTTO and J. P. LARPIN, *ibid.* **3** (1993) 309.
10. S. SEAL, S. K. BOSE and S. K. ROY, *Oxid. Met.* **41** (1994) 193.
11. H. BUSCAIL, C. COURTY and J. P. LARPIN, *J. Phys. IV* **5** (1995) 375.
12. B. A. PINT, *Oxid. Met.* **45** (1996) 1.
13. H. BUSCAIL and J. P. LARPIN, *Solid State Ionics* **92** (1996) 243.
14. E. CAUDRON, G. BAUD, J. P. BESSE, G. BLONDIAUX and M. JACQUET, *Solid State Ionics* **57** (1992) 189.
15. *Idem., Nucl. Instr. Meth.* **B83** (1993) 219.
16. *Idem., Solid State Ionics* **70/71** (1994) 629.
17. *Idem., Mat. Sci. Eng.* **B26** (1994) 181.
18. F. ROUX, G. BAUD, J. P. BESSE, E. CAUDRON and M. JACQUET, *Solid State Ionics* **104** (1997) 177.
19. K. PRZBYLSKI and G. J. YUREK, *Mat. Sci. Forum* **43** (1989) 1.
20. A. STRAWBRIDGE and P. Y. HOU, *Mat. High Temp.* **12** (1994) 177.
21. M. F. STROOSNIJDER, J. D. SUNDERKOTTER, M. J. CRISTOBAL and H. JENETT, *Surf. Coat. Tech.* **83** (1996) 205.
22. C. WAGNER, in "Atomic Movements" (American Society of Metallurgy, Cleveland, 1951) p. 153.
23. A. RAHMEL and W. SCHWENK, in "Korrosion und korrosionschutz von stahlen" (Verlag Chemie, Weinheim, 1977) p. 194.
24. P. HEMBREE and J. B. WAGNER, *Trans. AIME* **245** (1969) 1547.
25. P. KOFSTAD, in "High Temperature Corrosion" (Elsevier Applied Science, London, 1988) p. 68.
26. C. R. A. CATLOW, W. C. MACKRODT, M. J. NORGETT and A. M. STONEHAM, *Phil. Mag.* **A40** (1979) 161.
27. G. HETTICH, H. MEHRER and K. MAIER, *Scripta Metall.* **11** (1977) 795.

Received 13 September 1999
and accepted 22 February 2000